

Presurgical brain mapping in epilepsy using simultaneous EEG and functional MRI at ultra-high field: feasibility and first results

Frédéric Grouiller¹  · João Jorge^{2,3} · Francesca Pittau⁴ ·
Wietske van der Zwaag^{5,6} · Giannina Rita Iannotti⁷ · Christoph Martin Michel⁷ ·
Serge Vulliémoz⁴ · Maria Isabel Vargas⁸ · François Lazeyras¹

Received: 2 December 2015 / Revised: 11 February 2016 / Accepted: 12 February 2016
© ESMRMB 2016

Abstract

Objectives The aim of this study was to demonstrate that eloquent cortex and epileptic-related hemodynamic changes can be safely and reliably detected using simultaneous electroencephalography (EEG)–functional magnetic resonance imaging (fMRI) recordings at ultra-high field (UHF) for clinical evaluation of patients with epilepsy.

Materials and methods Simultaneous EEG–fMRI was acquired at 7 T using an optimized setup in nine patients with lesional epilepsy. According to the localization of the lesion, mapping of eloquent cortex (language and motor) was also performed in two patients.

Results Despite strong artifacts, efficient correction of intra-MRI EEG could be achieved with optimized artifact removal algorithms, allowing robust identification of interictal epileptiform discharges. Noise-sensitive topography-related analyses and electrical source localization were also performed successfully. Localization of epilepsy-related hemodynamic changes compatible with the lesion were detected in three patients and concordant with findings obtained at 3 T. Local loss of signal in specific regions, essentially due to B_1 inhomogeneities were found to depend on the geometric arrangement of EEG leads over the cap.

Conclusion These results demonstrate that presurgical mapping of epileptic networks and eloquent cortex is both safe and feasible at UHF, with the benefits of greater spatial resolution and higher blood-oxygenation-level-dependent sensitivity compared with the more traditional field strength of 3 T.

✉ Frédéric Grouiller
frederic.grouiller@unige.ch

¹ Department of Radiology and Medical Informatics, University of Geneva, Rue Gabrielle-Perret-Gentil 4, 1211 Geneva 14, Switzerland

² Laboratory for Functional and Metabolic Imaging, École Polytechnique Fédérale de Lausanne, Lausanne, Switzerland

³ ISR-Lisboa/LARSyS and Department of Bioengineering, Instituto Superior Técnico, Universidade de Lisboa, Lisbon, Portugal

⁴ EEG and Epilepsy Unit, Department of Neurology, Geneva University Hospitals, Geneva, Switzerland

⁵ Biomedical Imaging Research Center, Ecole Polytechnique Fédérale de Lausanne, Lausanne, Switzerland

⁶ Spinoza Centre for Neuroimaging, Amsterdam, The Netherlands

⁷ Functional Brain Mapping Laboratory, Department of Fundamental Neurosciences, University of Geneva, Geneva, Switzerland

⁸ Division of Neuroradiology, Geneva University Hospitals, Geneva, Switzerland

Keywords EEG–fMRI · Presurgical mapping · Epilepsy · Ultra-high field

Introduction

Functional magnetic resonance imaging (fMRI) is a non-invasive technique capable of detecting hemodynamic changes related to functional brain activity. The most widely used acquisition methods rely on the blood-oxygenation-level-dependent (BOLD) effect, which arises due to a local modification of the magnetic susceptibility caused by the paramagnetic properties of deoxyhemoglobin [1]. The ability to acquire fMRI at ultra-high field (UHF) offers the opportunity to greatly enhance BOLD contrast sensitivity and to subsequently improve the spatial resolution or decrease the number of events required to observe

a significant effect [2, 3]. Furthermore, the intravascular signal contribution from draining veins decreases with magnetic field strength [4], allowing a more accurate localization. These benefits open the possibility to better characterize epileptic networks using simultaneous electroencephalography (EEG) and to enhance our understanding of negative BOLD responses [5]. EEG–fMRI at UHF would permit more precise identification of epileptogenic areas and functional vital cortex during presurgical evaluations. Better EEG–fMRI sensitivity may be beneficial to patients with few interictal epileptiform discharges (IED) or those with mitigated results at 3 T.

However, the acquisition of EEG during fMRI, especially at UHF, suffers from various artifacts that compromise data quality. First, gradient artifacts completely obscure the EEG during fMRI acquisition. The rapid switching of magnetic field gradients produces electromagnetic induction into the loops formed by the wires of the EEG, the amplitude of which depends on gradient slew rates [6]. If EEG acquisition is synchronized with the MR clock, gradient artifacts are strictly periodic and reproducible and can easily be removed using moving average artifact template subtraction [7, 8]. Second, any motion or vibration of electrodes and leads in the static magnetic field produce induced electromotive forces in EEG that are proportional to the field strength [9]. In particular, pulse artifacts (PA), which are due to a combination of nodding head motion following each heartbeat, scalp expansion inducing motion of the electrodes near superficial arteries, and Hall effect produced by blood flow [10, 11], strongly contaminate the EEG. Contrary to gradient artifacts, PA are nonstationary and highly variable between successive heartbeats. The use of averaged artifact subtraction (AAS) is not sufficient to accurately remove PA, especially at higher fields [8, 12, 13], where both amplitude and variability greatly increase with magnetic field strength [14]. A second step using independent component analysis (ICA) [15] or optimal basis set (OBS) [16] is generally used to remove residuals. At UHF, vibrations induced by the helium pump [17] or by the ventilation system [18] could also seriously affect EEG quality, but they can be limited by using an optimized setup with ultrashort bundled wires [19]. Spontaneous head motion may also affect EEG recordings at higher field and compromise subsequent gradient and PA correction using moving average template subtraction. The fMRI realignment parameters can be used to improve gradient artifact removal [20], and piezoelectric sensors or additional loops on the EEG caps can be used to filter out motion artifacts [9, 21, 22].

Furthermore, the presence of EEG electrodes and conductive wires can alter the homogeneity of the static magnetic field (B_0) and disrupt the radiofrequency (RF) field (B_1), leading to local signal dropout and distortion in the vicinity of EEG electrodes and to a global decrease of signal-to-noise

ratio (SNR) [23]. These artifacts mainly depend on field strength and can significantly impact image quality at UHF. However, given that physiological noise is also reduced, temporal SNR of functional images is less affected, even in the presence of a dense-array EEG cap [24].

In addition to substantial artifacts, simultaneous recordings of EEG and fMRI at UHF raise important concerns regarding patient safety. First, the presence of EEG materials may alter the transmit B_1 field distribution, resulting in unpredicted local specific absorption rate (SAR) modification [25]. Second, the radiofrequency pulse wavelength decreases with static magnetic field intensity, increasing the risk of resonant antenna effects in the wires, especially at 7 T [26, 27].

In this report, preliminary results obtained in nine patients with epilepsy using simultaneous EEG–fMRI at 7 T are presented. Our aim was to demonstrate that using an optimized setup and appropriate artifacts removal algorithms, eloquent cortex and epileptic-related hemodynamic changes can be safely and reliably detected at UHF for clinical presurgical evaluation of epileptic patients. To our knowledge, this is the first report of simultaneous EEG–fMRI acquisition at UHF in patients with epilepsy.

Materials and methods

Patients

Nine epileptic patients with refractory lesional epilepsy were selected for simultaneous EEG and fMRI recordings at 7 T. For this study at UHF, patients with confirmed or strong suspicion of abnormalities of cortical development, who can benefit from structural imaging at higher field, were recruited. The frequency of IED was not an inclusion criterion. The exam had to be interrupted before simultaneous recording in two patients due to a focal seizure during structural imaging (patient 2) and to strong sensations of vertigo (patient 7). According to lesion localization, one patient also underwent a language fMRI (patient 9), and one completed a motor fMRI (patient 8) for presurgical mapping of eloquent cortex to be preserved during surgery. Clinical details for each patient are summarized in Table 1. All patients gave written informed consent, and the study was approved by the local ethics committee.

Data acquisition

Simultaneous EEG–fMRI

Simultaneous EEG–fMRI acquisitions were performed in a 7-T head-only scanner (Siemens Magnetom, Erlangen, Germany) equipped with an eight-channel transmit/receive

Table 1 Overview of clinical details and results of each patient

Patient	AE/gender/AO	Structural MRI	Interictal EEG (outside MRI)	Resection, iEEG	EEG-fMRI		Mapping of eloquent cortex
					EEG	fMRI	
1	31/M/1	L temporo-occipital FCD	P3 spikes	-	28 P3 spikes	Left mesio-occipital ($T_{\max} = 7.17$)	-
2	38/M/35	Normal	Independent F8-T4 and F7-T3 spikes	SEEG: bitemporal focus	Interrupted due to focal seizure during imaging	-	-
3	20/M/19	R > L frontal polymicrogyria	Normal	-	-	-	-
4	19/M/1	L frontal FCD	Bilateral frontocentral spikes	-	-	Bilateral fronto-temporal regions ($T_{\max} = 7.19$)	-
5	19/M/18	L temporal DNET	Normal	-	-	-	-
6	33/M/28	Normal	Normal	R postcentral FCD	-	-	-
7	23/F/18	R temporal DNET	-	-	Interrupted due to strong sensations of vertigo	-	-
8	32/M/17	R postcentral lesion of unknown origin	-	-	-	-	Motor
9A (7 T)	18/F/11	L temporo-occipital FCD	P7-T5 spikes	-	P7-T5 spikes, polyspikes, spikes-and-waves and abnormal theta and delta activity	Left posterior temporal ($T_{\max} = 6.88$)	Language
9B (3 T)					P7-T5 spikes, polyspikes, spikes-and-waves and abnormal theta and delta activity	Left posterior temporal ($T_{\max} = 5.51$)	Language

AE age at evaluation, AO age at onset, iEEG intracerebral electroencephalography, M male, F female, L left, R right, FCD focal cortical dysplasia, DNET dysembryoplastic neuroepithelial tumor

head RF coil (Rapid Biomedical, Rimpar, Germany) during 20 min at rest with eyes closed. All functional images were acquired using a T_2^* -weighted gradient-echo echo-planar imaging (GRE-EPI) sequence (TR = 2000 ms, TE = 25 ms, $\alpha = 78^\circ$, voxel size = $1.5 \times 1.5 \times 1.5\text{-mm}^3$, 32 axial slices with 1.5-mm interslice gaps).

An optimized EEG setup, with a customized 64-electrode cap (EasyCap, Herrsching, Germany) connected to two MR-compatible amplifiers (Brain Products, Gilching, Germany) via two ultra-short bundled cables, was used [19]. Each electrode lead included two 5 k Ω resistors—one near the electrode and one in the connector—to limit induced currents and thereby ensure patient safety [28]. EEG was acquired at 5 kHz synchronized with the 10-MHz MR clock to facilitate removal of gradient artifacts.

Patient 9 also had a simultaneous EEG–fMRI recording at 3 T (Siemens Prisma-Fit, Erlangen, Germany). Functional images were acquired using a 20-channel head coil with a GRE-EPI sequence (TR = 2000 ms, TE = 25 ms, $\alpha = 90^\circ$, voxel size = $3 \times 3 \times 3.75\text{-mm}^3$, 32 axial slices). EEG was recorded at 1-kHz with a 256-channel MR-compatible EEG (Electrical Geodesic Inc., Eugene, OR, USA).

Structural imaging

A $0.6 \times 0.6 \times 0.6\text{-mm}^3$ resolution MP2RAGE [29] and $0.4 \times 0.4 \times 1\text{-mm}^3$ resolution susceptibility-weighted imaging (SWI) were acquired for localization purposes in a separate session without EEG using a 32-channel head coil (Nova Medical, MA, USA).

Mapping of language and motor functions

Two runs for functional localization of the primary motor cortex of both hands were performed in patient 8. He was asked to open and close the hand (left or right) during four blocks of activation alternating with four blocks of rest, each with a duration of 24 s.

Patient 9 completed a language fMRI during which he listened to congruent and incongruent sentences for eight blocks of 24 s alternating with blocks of controls during which the same sentences were played backward [30]. For this patient, the same language task was performed at 3 T.

Data analysis

EEG preprocessing

Since most artifacts are proportional to the magnetic field and are much stronger at 7 T, gradient and PA correction is crucial to limit artifact residuals. The conventional artifact removal algorithms based on a template moving averaging using the neighboring occurrences of the artifact [7,

31] were adapted to avoid large artifacts, such as motion, entering into the template and contaminating the recording. Gradient artifacts were corrected using a moving average artifact subtraction method [7]. Nevertheless, median filtering is less sensitive to outliers than average filtering [32], and accordingly, the traditional averaging of L neighboring artifacts was replaced by a hybrid mean and median filtering to benefit from the strength of both methods. For each time point of the template, values of the L neighboring artifacts were sorted and the K minimal and maximal values removed from the averaging ($L = 30$, $K = 3$). This method allows exclusion of large outliers from the template and is much less sensitive to motion.

The EEG was then downsampled to 1 kHz, and PA were detected using an estimated ballistocardiogram signal calculated as the difference between the averaged EEG signals from a subset of 20 electrodes (FT9/FT10, TP9/TP10, FT7/FT8, T7/T8, TP7/TP8, F7/F8, AF7/AF8, F5/F6, FC5/FC6, C5/C6) located on the right and on the left temporal regions [33]. PA removal is generally performed using AAS that considers the preceding and following occurrences of the PA to be corrected [31]. However, PA are characterized by a great variability in amplitude and waveform between successive heartbeats, increasing with magnetic field intensity and giving rise to residuals after PA correction [14]. To deal with this important variability, we replaced the conventional moving averaging approach with a nonlocal mean (NLM) filtering [34] in which all PA occurrences were considered, with a weight depending on their similarity with the artifact instance to be corrected.

For each channel, the epochs of EEG are extracted around the PA peaks, resulting in a matrix X of dimensions $[N, T]$ where N is the number of PA occurrences and T is the number of time samples in the epochs. The epoch window was automatically adjusted for each patient to deal with heart-beat variability. The L_2 -norm $d_{i,j}$ between each pair of PA epochs stored in X was calculated. A weighting matrix was then built:

$$w_{i,j} = e^{-\frac{d_{i,j}^2}{\lambda^2}}$$

where λ is a filtering parameter set to 0.3.

Each PA was then estimated using NLM:

$$\widehat{PA}_i = \frac{\sum_{j=1}^N (w_{i,j} X_j)}{\sum_{j=1}^N w_{i,j}}$$

This method allows correcting the PA with less sensitivity to spontaneous head motion and to the high variability between successive PA occurrences. With this algorithm, the presence of residuals was negligible in comparison with the standard AAS correction (Fig. 1), and no additional step using ICA or OBS was required.

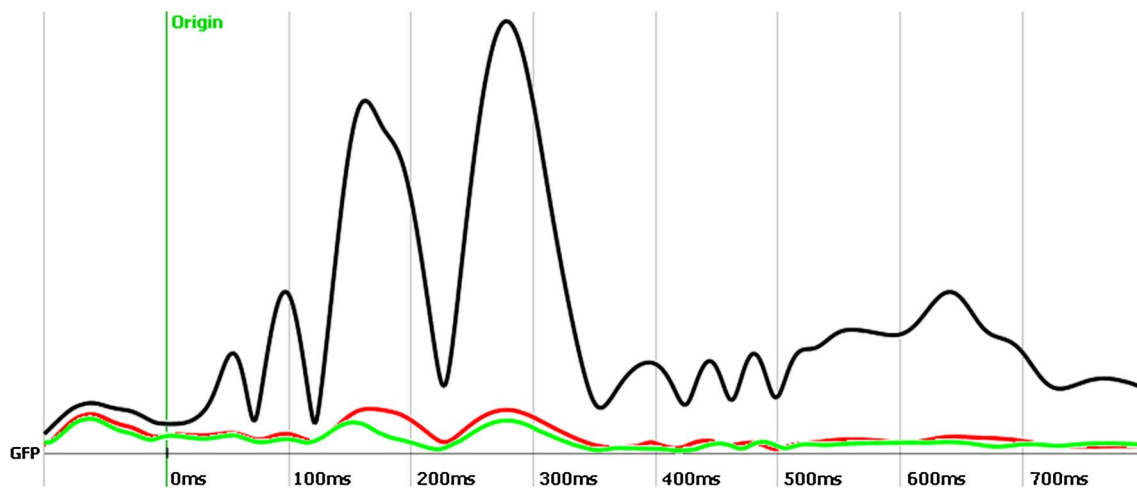


Fig. 1 Global field power of the averaged pulse artifact in one patient before correction (in *black*) after averaged artifact subtraction (AAS) (in *red*) and after nonlocal mean (NLM) averaging (in *green*). Residual artifacts after NLM correction are lower than after AAS correction

fMRI processing

All fMRI preprocessing and general linear model (GLM) analyses were performed using SPM8 (Wellcome Trust Centre for Neuroimaging, UCL, London, UK). Functional MRI images were motion-corrected, co-registered onto a high-resolution structural image, and spatially smoothed with an isotropic Gaussian kernel of 4 mm full width at half-maximum. Functional time series were analyzed voxel by voxel with a GLM. Low-frequency noise and signal drift were removed using a discrete cosine transform basis set with a filter cutoff period of 128 s. The six realignment parameters (R) and their Volterra expansion— $R_t R_t^2 R_{t-1} R_{t-1}^2$, where t and $t - 1$ refer, respectively, to the current and preceding timepoint [35]—were reduced using singular value decomposition (SVD). The N_C first SVD components explaining at least 99 % of the variance, or the first six SVD components if $N_C > 6$, were included into the GLM model as covariate regressors. This SVD reduction allows consideration of the 24 realignment parameters to remove any residual motion-related variance without decreasing too greatly the number of degrees of freedom while ensuring orthogonality of the model.

Spike-related and topography-related analyses

An experienced neurophysiologist visually detected IED in the corrected EEG. If no IED were recorded during the simultaneous EEG–fMRI session, a patient-specific epileptic topographic map was built by averaging IED detected in the clinical EEG acquired outside MRI. The presence of this epileptic topographic map in the intra-MRI EEG

was quantified by means of correlation-based fitting. IED timing or the time course of the topography-based correlation was then convolved with the canonical hemodynamic response function and used as a regressor for fMRI analysis [36]. IED-related or patient-specific topography-related hemodynamic changes were detected using a t test [$p < 0.05$, family-wise error (FWE) correction for multiple comparisons].

Electrical source imaging

Electrical source imaging (ESI) [37] was also performed with the interictal epileptic map using the freely available software Cartool (<https://sites.google.com/site/fbmlab/cartool>) [38] and compared with fMRI localization. Forward model was built using a locally spherical model with anatomical constraints (LSMAC) [38] based on the individual patient's high-resolution structural imaging. A linear-distributed inverse-solution algorithm with biophysical constraints was used to estimate the 3D current density distribution [39]. The EEG map at the 50 % rising phase of the averaged IED was considered for source analysis, as this timepoint localizes more accurately the underlying electrical source than the peak that already involves areas of spike propagation [40].

Motor and language mapping

For motor and language tasks, the block design was convolved with the canonical hemodynamic response function, and activated areas were identified using a GLM analysis ($p < 0.05$, family-wise correction for multiple comparisons).

Results

Spike-related and topography-related analyses

After optimized gradient and PA removal, the EEG was visually of excellent quality without noteworthy residuals. Despite PA of large amplitude and with a more complex waveform than at lower fields, IED could be identified after correction in two patients (patients 1 and 9, Fig. 2). In four patients, no IED were detected, even during the EEG acquired outside the MRI. For the last patient, rare IED were identified outside MRI and used to build an interictal topographical epileptic map (patient 4). Clinical details and results for each patient are summarized in Table 1.

Patient 1

After gradient and PA correction, 28 left parietal IED were identified in the EEG acquired during fMRI (Fig. 2). Structural MRI revealed a cortical and subcortical lesion, discretely hyperintense in the left temporo-occipital region on T2 and fluid-attenuated inversion recovery (FLAIRC) sequences, with a blurred differentiation between grey and white matter at 3 T, suggestive of a focal cortical dysplasia

and hyperintense on SWI at 7 T (Fig. 3a). IED-related BOLD changes were located in the left mesio-occipital cortex in concordance with the lesion (Fig. 3b). ESI was possible using the IED detected on the intra-MRI EEG and was located in the same region (Fig. 3c).

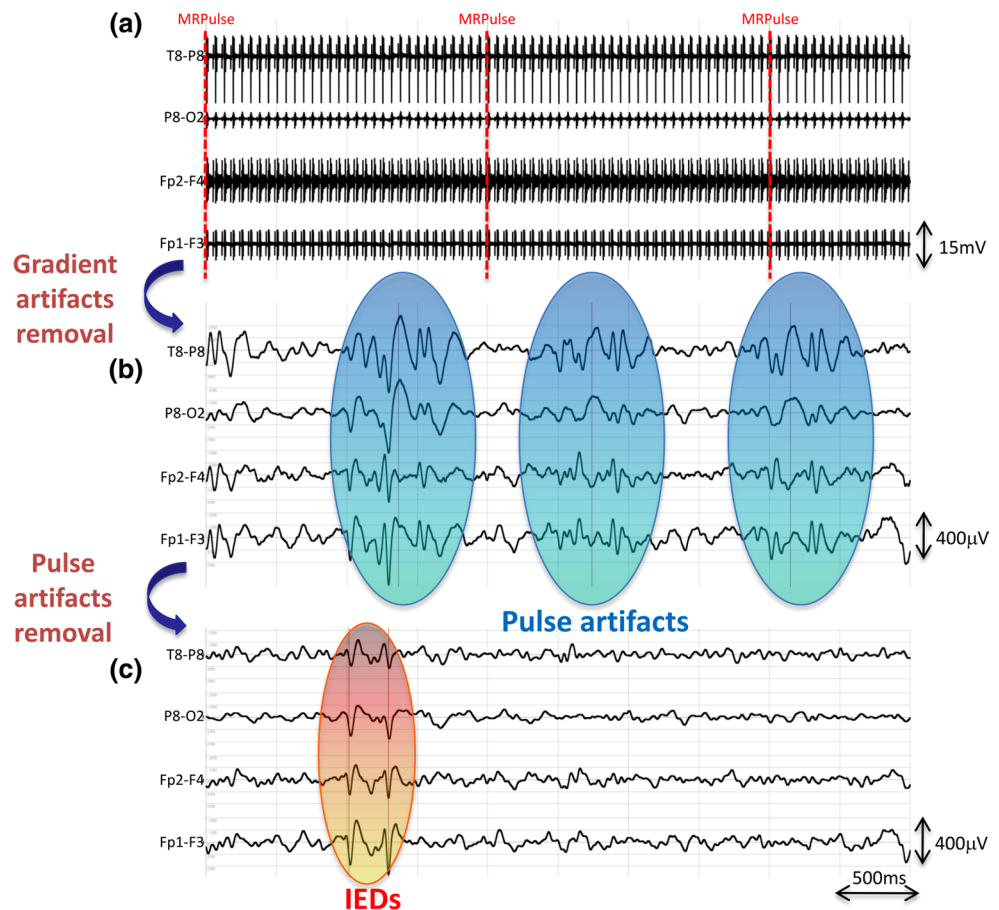
Patient 4

Left frontal dysplasia was identified in the structural imaging of this patient, whereas bilateral frontocentral IED was detected in the EEG recorded outside MRI. However, no IED were detected during simultaneous EEG–fMRI, and topography-related BOLD changes were located in bilateral frontotemporal areas using the interictal topographic map obtained outside MRI.

Patient 9

Structural imaging at 7 T revealed a small focal cortical dysplasia in left posterior temporal (Fig. 4a). Interictal EEG recorded outside and inside the MRI were characterized by very frequent spikes, polyspikes, spikes-and-wave, and abnormal theta and delta activity. We decided to perform topographical-related analysis to better model the

Fig. 2 Magnetic resonance (MR)-related artifact removal and electroencephalography (EEG) quality. **a** Raw EEG with gradient artifacts. **b** EEG after gradient artifact removal in the same time period. Pulse artifacts are highlighted in blue. **c** EEG after pulse artifact removal in the same time period. Interictal epileptiform discharges (IED), similar to the IED acquired outside the magnetic resonance imaging (MRI), are highlighted in red



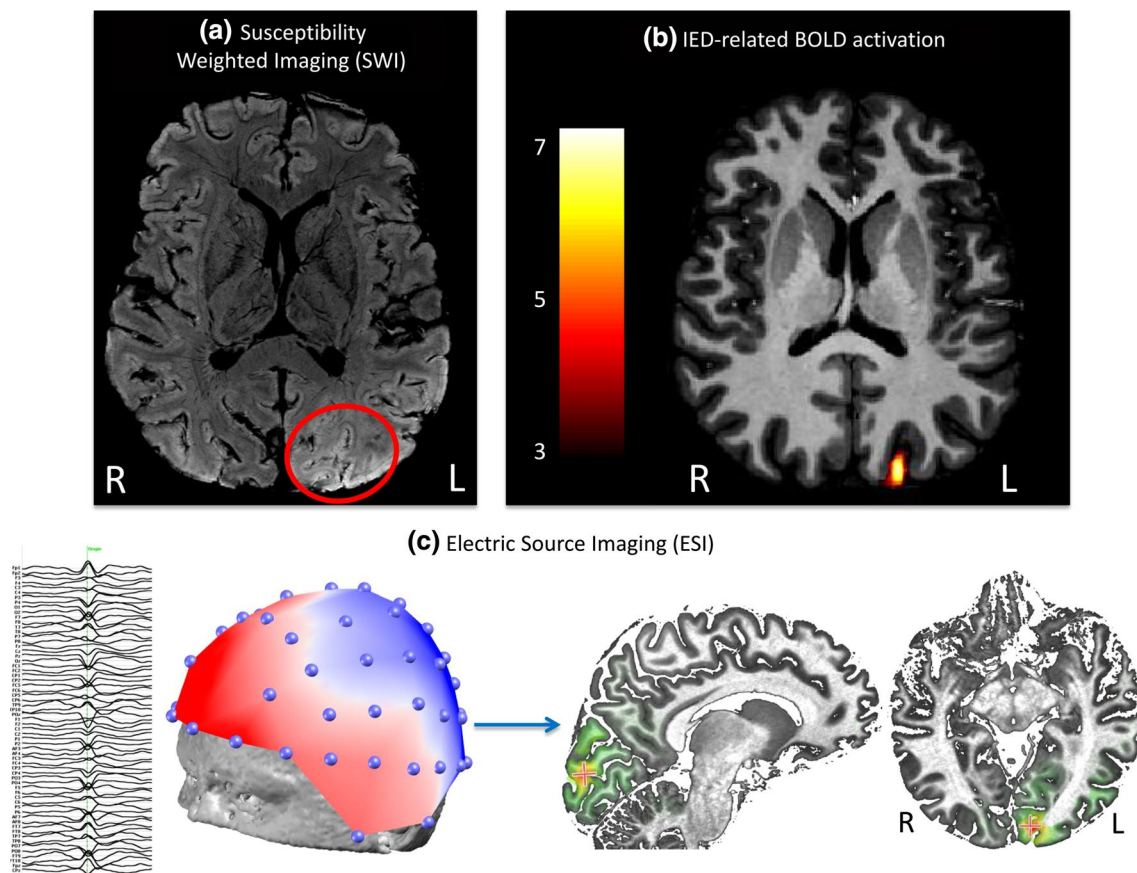


Fig. 3 Localization of interictal epileptic activity in patient 1. **a** Susceptibility-weighted imaging revealing a left mesio-occipital lesion (highlighted in red). **b** Interictal epileptiform discharge (IED)-related blood-oxygenation-level-dependent (BOLD) changes ($p < 0.001$, 20 voxels extent cluster, for visualization) in left mesio-occipital con-

cordant with the lesion. **c** *Left* intra-magnetic resonance imaging (MRI) IED averaging and corresponding scalp topographical map. *Right* electrical source imaging concordant with lesion and IED-related BOLD localizations

interictal epileptiform activity. The epileptic topographical map was obtained outside the MRI scanner using high-density EEG (Electrical Geodesics, Inc., 256 electrodes). This map allowed localization of epileptic sources with ESI in left temporal lobe (Fig. 4b) in concordance with the presence of the lesion. BOLD activation obtained with topography-related analysis using this same map was in the same area of the temporal lobe (Fig. 4c). For this patient, simultaneous EEG–fMRI was also acquired at 3 T with a different MR-compatible EEG (EGI, 256 electrodes). The topography-related analysis realized at 3 T produced positive BOLD changes accurately in the same location as 7 T but with a lower statistical power (Fig. 4c).

Localization of eloquent cortex

Patient 8

The motor fMRI realized in patient 8 did not produce any significant activation in the contralateral primary motor

cortex but only in the ipsilateral cerebellum. This can be explained by an important signal dropout in superior frontoparietal areas (Fig. 5a) due to the presence of the EEG connector and wires. The gradient-echo images and B_1^+ maps using a SA2RAGE sequence [41] in a phantom with the same 64-channel cap confirmed this finding (Fig. 5b). These B_1^+ inhomogeneities were found to be highly dependent on the geometric arrangement of conductive leads in the EEG cap. The use of another MR-compatible net (EGI, 256 electrodes, with the wires converging toward the back of the neck instead of the top of the head) also led to a general decrease in SNR yet produced a very different B_1^+ distribution (Fig. 5c).

Patient 9

The language fMRI performed in patient 9 revealed significant activation in the left inferior frontal gyrus and left temporal gyrus (Fig. 6a), concordant with previous localizations reported with this task [30]. The same task realized at

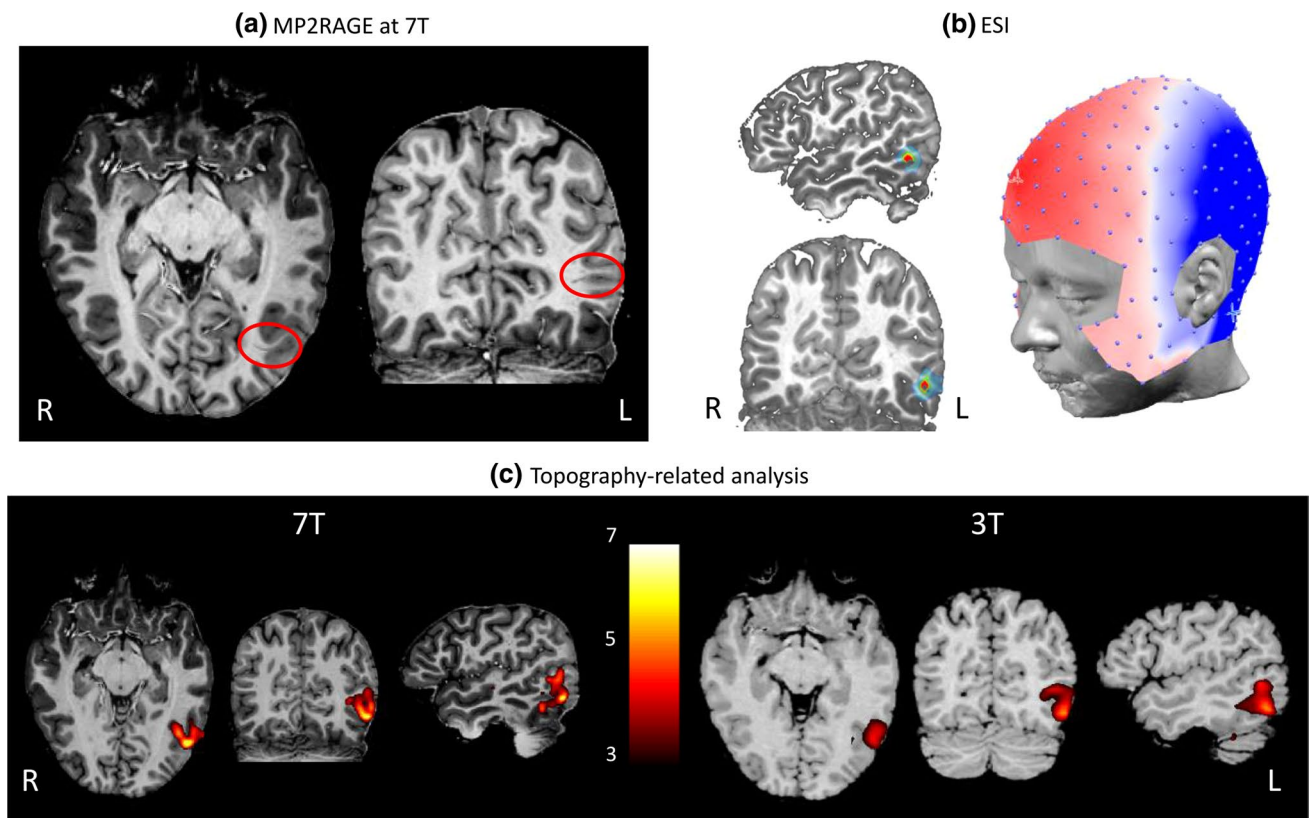


Fig. 4 Localization of interictal epileptic activity in patient 9. **a** High-resolution structural imaging (MP2RAGE), revealing a left temporal focal cortical dysplasia (highlighted in red). **b** Electrical source imaging realized using interictal epileptiform discharge (IED) recorded outside magnetic resonance imaging (MRI). The electric source is located in the left posterior middle temporal gyrus close to

the lesion. **c** Topography-related blood-oxygenation-level-dependent (BOLD) changes obtained by spatial correlation of the epileptic topographic map obtained outside functional MRI (fMRIC). BOLD changes ($p < 0.001$, 20 voxels extent cluster, for visualization) were located on the middle posterior temporal gyrus close to the lesion at 7 T (left) and 3 T (right)

3 T in the same patient produced activations strictly in the same areas, though with a lower statistical value (Fig. 6b).

Discussion

This work demonstrates the feasibility of recording simultaneous EEG–fMRI at 7 T in epileptic patients using an optimized setup that has been shown to decrease environment noise [19] and using modified artifact correction techniques to better remove artifact residuals (Fig. 1). After correcting gradient and PA, EEG quality allowed IED detection and the possibility of performing topography-related analysis. We also illustrate the possibility of complementing presurgical evaluation by oninvasive localization of eloquent cortex with fMRI.

Patient safety and comfort

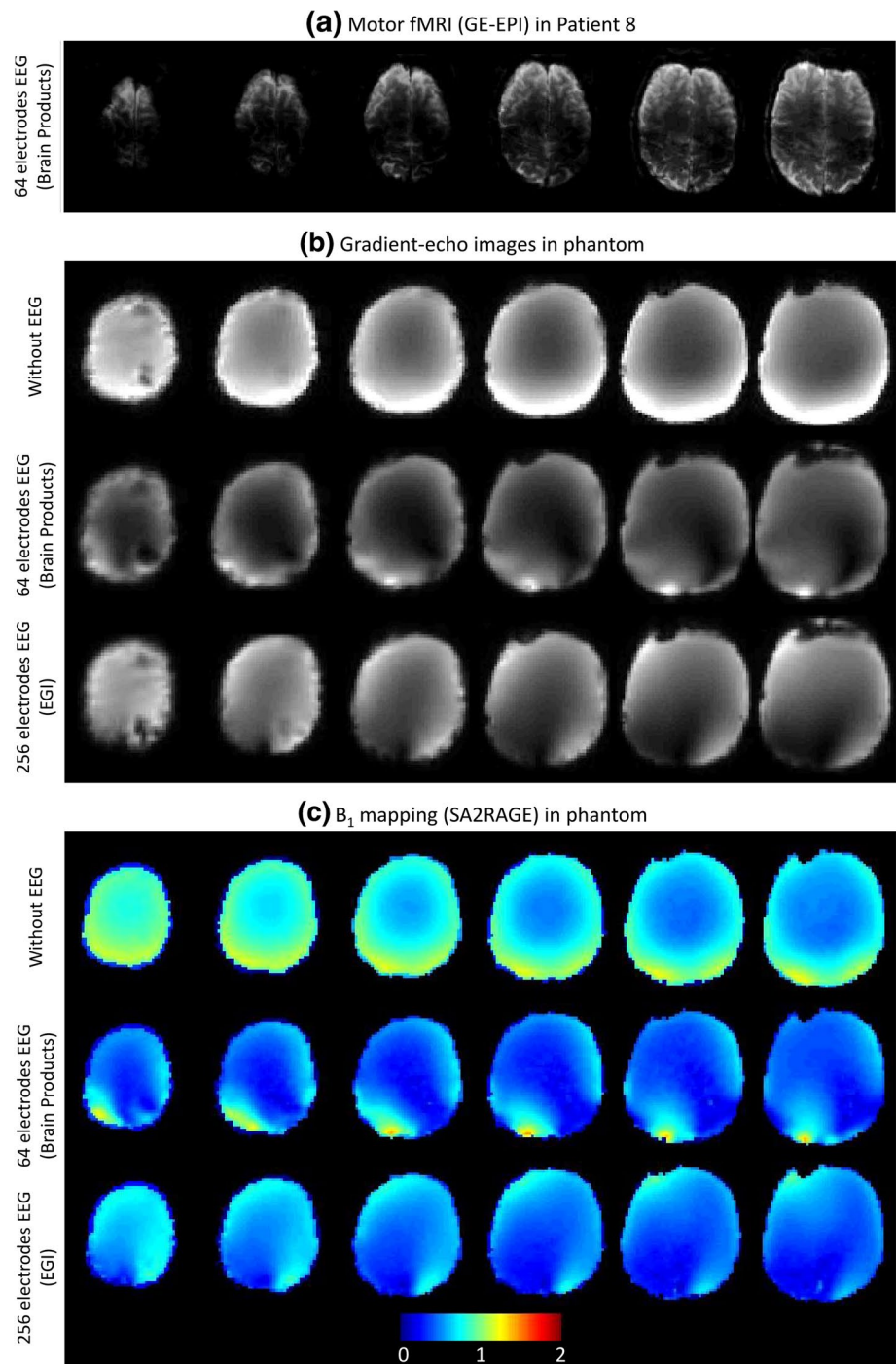
As already reported in a previous study on phantom and healthy individuals with this setup, no significant

temperature increases were found on EEG electrodes during simultaneous acquisition [19]. None of the patients reported any heating sensation or discomfort during the recordings. One patient had a focal seizure during structural imaging, and the exam was immediately interrupted for safety reasons. The risk of having a seizure in the MRI is not field-strength-dependent and may occur at lower field. We recruited patients who did not have frequent generalized tonic–clonic seizures, and medication was not modified before the exam. Another patient complained of vertigo when she was moved into the magnetic field. Adverse side effects such as nausea, vertigo, metallic taste in the mouth, or light flashes are increased at UHF compared with lower field but are generally well tolerated [42] and not specific to this patient population.

MRI-related artifact removal

The optimized setup with ultra-short bundled wires used in this work allows a significant reduction in environment noise contributions, due to vibrations, that result in

Fig. 5 Functional image quality in the presence of electroencephalography (EEG). **a** Functional images [gradient-echo echo-planar imaging (GRE-EPI)] during motor functional magnetic resonance imaging (fMRI) in patient 8. Important signal losses are visible in superior frontocentral areas. **b** GRE images in a phantom without EEG (*upper row*), with 64-channel Brain Products system (*middle row*) and with 256-channel EGI system (*lower row*). Signal losses are located in upper axial slices with Brain Amp system, whereas they are located in posterior regions with EGI system. **c** B_1^+ maps obtained with SA2RAGE sequence without EEG (*upper row*), with 64-channel Brain Products system (*middle row*) and with 256-channel EGI system (*lower row*). B_1^+ field distributions are expressed as a fraction of the nominal flip angle



important artifacts at UHF [19]. In order to be less sensitive to motion artifacts, we used a hybrid mean and median moving-average algorithm to remove gradient artifacts. Thanks to synchronization of the EEG acquisition with the MR clock, these artifacts were successfully corrected. PA at UHF are characterized by a large amplitude and great variability between successive heartbeats. To deal with this nonstationarity, we implemented an NLM algorithm that removed PA successfully with less residuals than using conventional AAS (Fig. 1). Given that the corrected EEG

was of good quality, without visible residuals, a second step using ICA or OBS was not required, thus decreasing the processing time and making the artifact correction pipeline fully transposable for real-time processing.

EEG–fMRI combination

After MR-artifact removal, IED were identified in the intra-MRI EEG, and hemodynamic changes related to this interictal activity were successfully detected. Epileptic

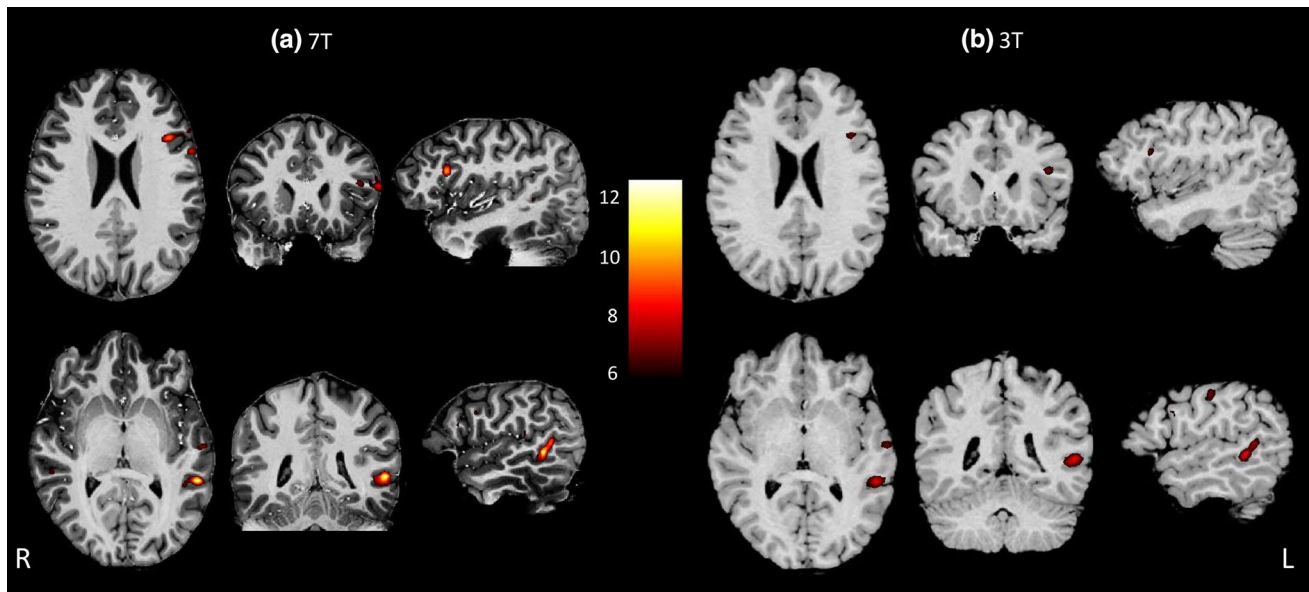


Fig. 6 Presurgical language mapping using functional magnetic resonance imaging (fMRI) in patient 9 [$p < 0.05$, family-wise error (FWE) correction] at **a** 7 T and **b** 3 T. Blood-oxygenation-level-

dependent (BOLD) activations were obtained in left inferior frontal gyrus and left superior temporal gyrus at 3 T and 7 T

source localization was performed with these intra-MRI IED, allowing for a better spatiotemporal localization of interictal epileptic activity [43, 44]. In case of absence or rare interictal events, a topographic epileptic map obtained outside MRI can be used to detect hemodynamic changes related to interictal activity [36]. This type of topographical analysis is very sensitive to noise, such as PA residuals or motion. The concordant localization of epileptic activity with this method, according to the lesion in structural images, demonstrates outstanding corrected EEG quality.

Mapping of eloquent cortex

Very few studies have reported fMRI results from patients at UHF [45, 46]. In our study, language or motor fMRI were proposed for presurgical mapping of eloquent cortex in patients in whom the lesion was potentially close to these areas, which were to be preserved during surgery. The language network, including temporal–parietal junction and inferior frontal areas, was successfully mapped in one patient. In contrast, the motor primary cortex could not be mapped in a second patient due to strong local signal dropouts caused by EEG wires and connectors. Presurgical mapping of functional cortex can be realized at UHF but should be done preferably without EEG electrodes. Even in this case, attention should be paid to local susceptibility-related artifacts, especially in inferior frontal regions, to avoid false negatives [45].

Image quality

The presence of the EEG system results in a global SNR loss, although functional images are affected less than structural images [19, 24]. Local susceptibility artifacts due to the presence of electrodes were limited to the skull and did not affect the brain. However, B_1^+ maps were strongly affected by the presence of EEG electrodes and leads. This resulted in important signal dropout in specific regions, depending on the EEG cap configuration. The signal dropout in the superior frontocentral region using the 64-channel Brain Products EEG compromised detection of hemodynamic changes in primary motor cortex for patient 8. However, the B_1^+ map obtained using a 256-channel EGI system on a phantom revealed a different distribution, with signal losses mostly in parieto-occipital regions. Depending on the brain region of interest, the choice of EEG cap layout could be crucial. Possible improvements include cap design modification to obtain a homogenous field distribution or the use of an EEG cap based on conductive ink technology (InkCap) that permits improvement of image quality during simultaneous recordings [47].

Comparison with 3 T

The topography-related BOLD changes obtained at 3 T and 7 T in patient 9 were located consistently and rigorously in the same brain area near the lesion, attesting to good reproducibility across field strengths, as already shown by

comparing 1.5 T and 3 T [48]. BOLD sensitivity obtained at 7 T is known to be greater than at 3 T, but this comparison is particularly difficult in the case of spontaneous activity such as in epilepsy because it may vary greatly between recordings depending on the epileptic activity (number of IED events, for instance). The language localization performed both at 3 T and 7 T in the same patient revealed the same networks, but sensitivity was greatly enhanced at higher field (Fig. 6). A comparison with a greater number of patients is needed to confirm these findings, though the increase in BOLD sensitivity with field strength itself has been shown many times in various brain regions [2, 3].

Clinical feasibility and relevance

Despite its various benefits, the role of UHF MRI in clinical contexts is still a topic of debate. These preliminary results demonstrate that simultaneous EEG–fMRI at UHF could be used safely to map epileptic networks. This non-invasive presurgical mapping can be complemented by localization of eloquent cortex using fMRI with a greater sensitivity. This opens the opportunity to increase spatial resolution, improving localization and spatial specificity; or to decrease the experiment duration, increasing efficiency. Overall, the possibility to record EEG–fMRI at UHF opens new perspectives to better characterize epileptic networks and may thus prove highly relevant for both fundamental research and clinical practice.

Conclusion

Epileptic network and functional eloquent cortex localizations using an optimized EEG–fMRI setup and artifact removal algorithms can be performed safely at UHF. EEG quality allows noise-sensitive analyses such as EEG topography spatial correlation, yielding precise localization of correlated hemodynamic changes. B_1^+ inhomogeneities are highly dependent on the choice of EEG cap and could potentially be reduced in regions of interest by adapting the layout of the wires. These results open new perspectives to better characterize epileptic networks at higher field, with greater spatial resolution and better BOLD sensitivity than at 3 T, and could be beneficial for patients having mitigated results obtained with clinical MRI available today.

Acknowledgments This work was supported by the Swiss National Science Foundation for Scientific Research (Grants 326030-150816, 33CM30-140332, 320030-141165 and 146633), by the Department of Radiology of Geneva University Hospitals (startup Grant 2013-10), and by the Center for Biomedical Imaging (CIBM) of the Universities and Hospitals of Geneva and Lausanne, and the EPFL.

Compliance with the ethical standards

Conflict of interest The authors declare that they have no conflict of interest.

Research involving human participants All procedures performed in this study were in accordance with the ethical standards of the institutional and research committee and with the 1964 Declaration of Helsinki and its later amendments.

Informed consent Informed consent was obtained from all participants in the study.

References

- Ogawa S, Tank DW, Menon R, Ellermann JM, Kim SG, Merkle H, Ugurbil K (1992) Intrinsic signal changes accompanying sensory stimulation: functional brain mapping with magnetic resonance imaging. *Proc Natl Acad Sci USA* 89(13):5951–5955
- Turner R, Jezzard P, Wen H, Kwong KK, Le Bihan D, Zeffiro T, Balaban RS (1993) Functional mapping of the human visual cortex at 4 and 1.5 tesla using deoxygenation contrast EPI. *Magn Reson Med* 29(2):277–279
- van der Zwaag W, Francis S, Head K, Peters A, Gowland P, Morris P, Bowtell R (2009) fMRI at 1.5, 3 and 7 T: characterising BOLD signal changes. *Neuroimage* 47(4):1425–1434
- Duong TQ, Yacoub E, Adriany G, Hu X, Ugurbil K, Kim SG (2003) Microvascular BOLD contribution at 4 and 7 T in the human brain: gradient-echo and spin-echo fMRI with suppression of blood effects. *Magn Reson Med* 49(6):1019–1027
- Bianciardi M, Fukunaga M, van Gelderen P, de Zwart JA, Duyn JH (2011) Negative BOLD-fMRI signals in large cerebral veins. *J Cereb Blood Flow Metab* 31(2):401–412
- Felblinger J, Slotboom J, Kreis R, Jung B, Boesch C (1999) Restoration of electrophysiological signals distorted by inductive effects of magnetic field gradients during MR sequences. *Magn Reson Med* 41(4):715–721
- Allen PJ, Josephs O, Turner R (2000) A method for removing imaging artifact from continuous EEG recorded during functional MRI. *Neuroimage* 12(2):230–239
- Grouiller F, Vercueil L, Krainik A, Segebarth C, Kahane P, David O (2007) A comparative study of different artefact removal algorithms for EEG signals acquired during functional MRI. *Neuroimage* 38(1):124–137
- Jorge J, Grouiller F, Gruetter R, van der Zwaag W, Figueiredo P (2015) Towards high-quality simultaneous EEG–fMRI at 7T: detection and reduction of EEG artifacts due to head motion. *Neuroimage* 120:143–153
- Mullinger KJ, Havenhand J, Bowtell R (2013) Identifying the sources of the pulse artefact in EEG recordings made inside an MR scanner. *Neuroimage* 71:75–83
- Yan WX, Mullinger KJ, Geirsdottir GB, Bowtell R (2010) Physical modeling of pulse artefact sources in simultaneous EEG/fMRI. *Hum Brain Mapp* 31(4):604–620
- Vanderperren K, De Vos M, Ramautar JR, Novitskiy N, Mennes M, Assecondi S, Vanrumste B, Stiers P, Van den Bergh BR, Wagemans J, Lagae L, Sunaert S, Van Huffel S (2010) Removal of BCG artifacts from EEG recordings inside the MR scanner: a comparison of methodological and validation-related aspects. *Neuroimage* 50(3):920–934
- Arrubla J, Neuner I, Dammers J, Breuer L, Warbrick T, Hahn D, Poole MS, Boers F, Shah NJ (2014) Methods for pulse artefact

- reduction: experiences with EEG data recorded at 9.4 T static magnetic field. *J Neurosci Methods* 232:110–117
14. Debener S, Mullinger KJ, Niazy RK, Bowtell RW (2008) Properties of the ballistocardiogram artefact as revealed by EEG recordings at 1.5, 3 and 7 T static magnetic field strength. *Int J Psychophysiol* 67(3):189–199
 15. Debener S, Strobel A, Sorger B, Peters J, Kranczioch C, Engel AK, Goebel R (2007) Improved quality of auditory event-related potentials recorded simultaneously with 3-T fMRI: removal of the ballistocardiogram artefact. *Neuroimage* 34(2):587–597
 16. Niazy RK, Beckmann CF, Iannetti GD, Brady JM, Smith SM (2005) Removal of fMRI environment artifacts from EEG data using optimal basis sets. *Neuroimage* 28(3):720–737
 17. Rothlubbers S, Relvas V, Leal A, Figueiredo P (2013) Reduction of EEG artefacts induced by vibration in the MR-environment. *Conf Proc IEEE Eng Med Biol Soc* 2013:2092–2095
 18. Nierhaus T, Gundlach C, Goltz D, Thiel SD, Pleger B, Villringer A (2013) Internal ventilation system of MR scanners induces specific EEG artifact during simultaneous EEG–fMRI. *Neuroimage* 74:70–76
 19. Jorge J, Grouiller F, Ipek O, Stoermer R, Michel CM, Figueiredo P, van der Zwaag W, Gruetter R (2015) Simultaneous EEG–fMRI at ultra-high field: artifact prevention and safety assessment. *Neuroimage* 105:132–144
 20. Moosmann M, Schonfelder VH, Specht K, Scheeringa R, Nordby H, Hugdahl K (2009) Realignment parameter-informed artefact correction for simultaneous EEG–fMRI recordings. *Neuroimage* 45(4):1144–1150
 21. Bonmassar G, Purdon PL, Jaaskelainen IP, Chiappa K, Solo V, Brown EN, Belliveau JW (2002) Motion and ballistocardiogram artifact removal for interleaved recording of EEG and EPs during MRI. *Neuroimage* 16(4):1127–1141
 22. Masterton RA, Abbott DF, Fleming SW, Jackson GD (2007) Measurement and reduction of motion and ballistocardiogram artefacts from simultaneous EEG and fMRI recordings. *Neuroimage* 37(1):202–211
 23. Mullinger K, Debener S, Coxon R, Bowtell R (2008) Effects of simultaneous EEG recording on MRI data quality at 1.5, 3 and 7 tesla. *Int J Psychophysiol* 67(3):178–188
 24. Luo Q, Glover GH (2012) Influence of dense-array EEG cap on fMRI signal. *Magn Reson Med* 68(3):807–815
 25. Angelone LM, Pothast A, Segonne F, Iwaki S, Belliveau JW, Bonmassar G (2004) Metallic electrodes and leads in simultaneous EEG–MRI: specific absorption rate (SAR) simulation studies. *Bioelectromagnetics* 25(4):285–295
 26. Dempsey MF, Condon B, Hadley DM (2001) Investigation of the factors responsible for burns during MRI. *J Magn Reson Imaging* 13(4):627–631
 27. Schick F (2005) Whole-body MRI at high field: technical limits and clinical potential. *Eur Radiol* 15(5):946–959
 28. Lemieux L, Allen PJ, Franconi F, Symms MR, Fish DR (1997) Recording of EEG during fMRI experiments: patient safety. *Magn Reson Med* 38(6):943–952
 29. Marques JP, Kober T, Krueger G, van der Zwaag W, Van de Moortele PF, Gruetter R (2010) MP2RAGE, a self bias-field corrected sequence for improved segmentation and T1-mapping at high field. *Neuroimage* 49(2):1271–1281
 30. Genetti M, Grouiller F, Vuillemoz S, Spinelli L, Seeck M, Michel CM, Schaller K (2013) Noninvasive language mapping in patients with epilepsy or brain tumors. *Neurosurgery* 72(4):555–565
 31. Allen PJ, Polizzi G, Krakow K, Fish DR, Lemieux L (1998) Identification of EEG events in the MR scanner: the problem of pulse artifact and a method for its subtraction. *Neuroimage* 8(3):229–239
 32. Sijbers J, Van Audekerke J, Verhoye M, Van der Linden A, Van Dyck D (2000) Reduction of ECG and gradient related artifacts in simultaneously recorded human EEG/MRI data. *Magn Reson Imaging* 18(7):881–886
 33. Iannotti GR, Pittau F, Michel CM, Vuillemoz S, Grouiller F (2015) Pulse artifact detection in simultaneous EEG–fMRI recording based on EEG map topography. *Brain Topogr* 28(1):21–32
 34. Buades A, Coll B, Morel JM (2005) A review of image denoising algorithms, with a new one. *Multiscale Model Simul* 4(2):490–530
 35. Friston KJ, Williams S, Howard R, Frackowiak RS, Turner R (1996) Movement-related effects in fMRI time-series. *Magn Reson Med* 35(3):346–355
 36. Grouiller F, Thornton RC, Groening K, Spinelli L, Duncan JS, Schaller K, Siniatchkin M, Lemieux L, Seeck M, Michel CM, Vuillemoz S (2011) With or without spikes: localization of focal epileptic activity by simultaneous electroencephalography and functional magnetic resonance imaging. *Brain* 134(Pt 10):2867–2886
 37. Michel CM, Murray MM, Lantz G, Gonzalez S, Spinelli L, Grave de Peralta R (2004) EEG source imaging. *Clin Neurophysiol* 115(10):2195–2222
 38. Brunet D, Murray MM, Michel CM (2011) Spatiotemporal analysis of multichannel EEG: CARTOOL. *Comput Intell Neurosci* 2011:813870
 39. de Peralta Grave, Menendez R, Murray MM, Michel CM, Martuzzi R, Gonzalez Andino SL (2004) Electrical neuroimaging based on biophysical constraints. *Neuroimage* 21(2):527–539
 40. Lantz G, Spinelli L, Seeck M, de Peralta Menendez RG, Sottas CC, Michel CM (2003) Propagation of interictal epileptiform activity can lead to erroneous source localizations: a 128-channel EEG mapping study. *J Clin Neurophysiol* 20(5):311–319
 41. Eggenschwiler F, Kober T, Magill AW, Gruetter R, Marques JP (2012) SA2RAGE: a new sequence for fast B₁⁺-mapping. *Magn Reson Med* 67(6):1609–1619
 42. Theysohn JM, Maderwald S, Kraff O, Moeninghoff C, Ladd ME, Ladd SC (2008) Subjective acceptance of 7 Tesla MRI for human imaging. *Magn Reson Mater Phys* 21(1–2):63–72
 43. Groening K, Brodbeck V, Moeller F, Wolff S, van Baalen A, Michel CM, Jansen O, Boor R, Wiegand G, Stephani U, Siniatchkin M (2009) Combination of EEG–fMRI and EEG source analysis improves interpretation of spike-associated activation networks in paediatric pharmacoresistant focal epilepsies. *Neuroimage* 46(3):827–833
 44. Vuillemoz S, Thornton R, Rodionov R, Carmichael DW, Guye M, Lhatoo S, McEvoy AW, Spinelli L, Michel CM, Duncan JS, Lemieux L (2009) The spatio-temporal mapping of epileptic networks: combination of EEG–fMRI and EEG source imaging. *Neuroimage* 46(3):834–843
 45. Geissler A, Matt E, Fischmeister F, Wurnig M, Dymerska B, Knosp E, Feucht M, Trattig S, Auff E, Fitch WT, Robinson S, Beisteiner R (2014) Differential functional benefits of ultra high-field MR systems within the language network. *Neuroimage* 103:163–170
 46. Beisteiner R, Robinson S, Wurnig M, Hilbert M, Merksa K, Rath J, Hollinger I, Klinger N, Marosi C, Trattig S, Geissler A (2011) Clinical fMRI: evidence for a 7T benefit over 3T. *Neuroimage* 57(3):1015–1021
 47. Vasios CE, Angelone LM, Purdon PL, Ahveninen J, Belliveau JW, Bonmassar G (2006) EEG/(f)MRI measurements at 7 Tesla using a new EEG cap (“InkCap”). *Neuroimage* 33(4):1082–1092
 48. Gholipour T, Moeller F, Pittau F, Dubeau F, Gotman J (2011) Reproducibility of interictal EEG–fMRI results in patients with epilepsy. *Epilepsia* 52(3):433–442